Engineering with Computers (2021) 37:1765–1779
https://doi.org/10.1007/s00366-019-00910-1

ORIGINAL ARTICLE

Implementation of periodic boundary conditions for loading of mechanical metamaterials and other complex geometric microstructures using finite element analysis

Luke Mizzi[1] · Daphne Attard[1] · Ruben Gatt[1] · Krzysztof K. Dudek[1,2] · Brian Ellul[1] · Joseph N. Grima[1,3]

Received: 15 February 2019 / Accepted: 16 December 2019 / Published online: 1 January 2020

Abstract
The implementation of periodic boundary conditions (PBCs) is one of the most important and difficult steps in the computational analysis of structures and materials. This is especially true in cases such as mechanical metamaterials which typically possess intricate geometries and designs which makes finding and implementing the correct PBCs a difficult challenge. In this work, we analyze one of the most common PBCs implementation technique, as well as implement and validate an alternative generic method which is suitable to simulate any possible 2D microstructural geometry with a quadrilateral unit cell regardless of symmetry and mode of deformation. A detailed schematic of how both these methods can be employed to study 3D systems is also presented.

Keywords Finite element analysis · Mechanical metamaterials · Periodic boundary conditions · Auxetics · Mechanical properties

1 Introduction

Mechanical metamaterials are systems whose mechanical properties are governed primarily by their structural framework rather than material composition. In recent years, there have been numerous studies on these materials, which represent a novel class of systems in the field of material science. This interest has arisen mainly due to their versatility and ability to exhibit a wide range of mechanical properties, particularly negative properties such as negative Poisson's ratio (auxeticity) [1–7], negative stiffness [8] and negative compressibility [9–11], which are not commonly found in conventional materials.

The finite element (FE) method is one of the most common techniques used to study these systems. Mechanical metamaterials typically possess intricate geometries which are repeated multiple times to form a sheet or block of material. The standard modus operandi used to study these systems takes advantage of this, by employing the use of the representative area or volume elements (RVEs) with periodic boundary conditions to simulate the deformation behaviour of these systems [12–23]. This allows one to study stress and strain fields and distributions as well as investigate the mechanical properties of these systems. These representative elements typically consist of one or multiple repeating units, depending on the type of analysis required. The periodic boundary conditions (PBCs) method entails the simulation of a structure as an infinite system with all pairs of opposing boundaries (two or three depending on whether the system is 2D or 3D, respectively) deforming in an identical manner, thus creating a scenario where edge or boundary effects are completely eliminated. Although it is well known that in real life all materials have boundaries and, thus, in reality edge effects will always play some role on the deformation of the system, one may also argue that should a finite system possess a sufficiently large number of repeating units then it will deform similarly to an infinite system. This reasoning is based upon the assumption that in a system with a very large number of repeating units, the ratio of boundary units to internal units is extremely low and therefore the overall

✉ Luke Mizzi
luke.mizzi@um.edu.mt; luke.mizzi@unimore.it

[1] Metamaterials Unit, Faculty of Science, University of Malta, MSD 2080, Msida, Malta

[2] Institute of Physics, University of Zielona Gora, ul. Szafrana 4a, 65-069 Zielona Gora, Poland

[3] Department of Chemistry, Faculty of Science, University of Malta, MSD 2080, Msida, Malta

deformation behaviour and, hence, mechanical properties of the system will be determined by the deformation of the internal units forming the bulk material. This approach is considered as an ideal method to investigate large patterned systems with periodic representative elements using minimal computational resources and time.

However, the validity of the PBCs method hinges upon the proper implementation of the boundary conditions at the edges of the representative area element or unit cell of, as well as the constraints used to avoid rigid body motion and applied loads. Here it is important to note that the implementation of periodicity to a system or structure does not necessarily entail a resultant accurate picture of the actual deformation of the unit cell in a large finite system, i.e. a system may deform periodically but be still deforming in an incorrect manner. Improper boundary conditions which overly constrain the system or inhibit it from deforming in its natural manner would result in unrealistic deformations which do not reflect in any way the actual behaviour of the system in real life. Also, while certain boundary conditions which may be sufficient to simulate certain geometries, they may not be suited to other systems which deform in a more complex manner and systems with asymmetric repeating unit geometries [24–26]. In these cases, finding or devising the correct method to simulate these systems can be an arduous undertaking, especially if the system in question is a novel design which has never been studied before. This problem is particularly pertinent in the case of mechanical metamaterials, which due to their intricate and often highly porous geometries, present a considerable challenge in this regard.

In view of this, in this paper, we present a PBCs method which may be used to simulate any 2D mechanical metamaterial based on a quadrilateral unit cell, regardless of geometry. This method was validated on a number of auxetic mechanical metamaterial geometries with well-known mechanical properties and deformation mechanisms. In addition, we also discuss how the same reasoning and methodology may be applied to simulate 3D systems. We also investigate how the characteristics and symmetry conditions of certain geometries may allow them to be successfully simulated using other PBCs methods which are relatively easier to implement.

2 Periodic boundary conditions

2.1 Periodicity

Before discussing the methods through which PBCs can be applied to simulate mechanical metamaterial geometries, it is important to first define what constitutes a periodic unit cell with correct PBCs. The two main criteria employed to define a periodic unit cell are:

1. The relative displacement of elements at the boundaries of the simulated cell following loading are identical to those on the corresponding opposing boundaries and;
2. Regardless of the number of repeating units/unit cells used to define the simulated cell, the deformation profile and mechanical properties of the system must remain unchanged.

The first criterion ensures that the geometry of the system remains periodic throughout deformation. The second condition, on the other hand, ensures the validity of the PBCs for simulating the system. If the PBCs are imposing any artificial constraints on the system then the repeating units on the edges of the simulated cell would deform differently than those at the centre and thus the mechanical properties of the system would be influenced by the number of repeating units. However, if the PBCs are correctly applied, then the number of repeating units in the simulated cell should have no bearing on its deformation, and thus the simulated cell's behaviour represents that of a corresponding infinite system.

2.2 Periodic boundary conditions applied through fixes and strains (Method 1)

There are several methods which one can use to ensure that the boundaries of a simulated cell deform in an identical manner. One of the most commonly employed methods in FE analysis is to use fixes and strains to constrain the simulated cell to retain its original shape. This is typically done in the manner shown in Fig. 1, where a system with a rectangular unit cell is simply supported from the nodes at one of the horizontal and vertical edges of the cell, a fixed displacement is applied on the side from which the system is loaded and the displacements in the y direction of the nodes on the remaining edge Xb are coupled in order to ensure that it remains straight. Therefore, the allowed displacement of the nodes at the two horizontal and vertical edges of the cell (Xa, Xb and Ya, Yb, respectively) in the x- and y-directions (UX and UY, respectively) may be defined as follows:

Xa $UX = \text{Free}$, $UY = 0$

Ya $UX = 0$, $UY = \text{Free}$

Xb $UX = \text{Free}$, UY of all nodes on this edge is equal but the overall magnitude and direction of UY is unrestricted

Yb $UX = \delta l_x$ where $\delta l_x = l_x \varepsilon_x$, with l_x represents the original length of sides Xa and Xb and ε_x is the applied strain on the unit cell in the x-direction, $UY = \text{Free}$

This method for applying PBCs allows the simulated cell two degrees of freedom during deformation, δl_x and

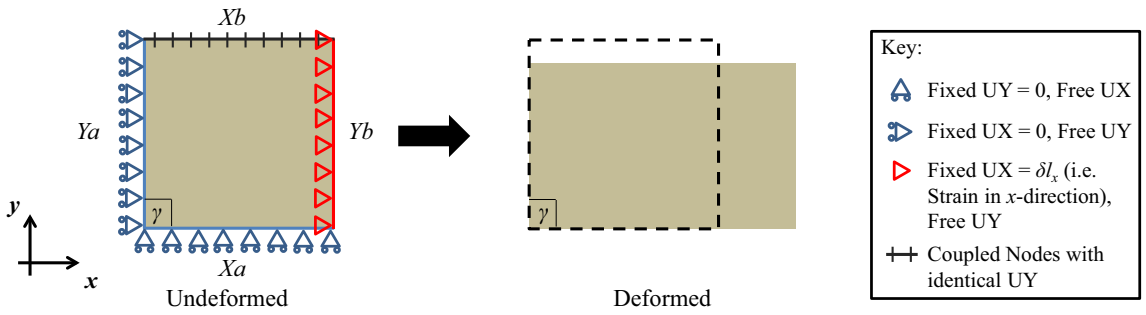

Fig. 1 Diagram depicting the application of PBCs and loading in the *x*-direction of a system with a quadratic unit cell through the use of fixed displacement and strains. Both fixes and strains control the displacement of the edge nodes in the *x*- (*UX*) and *y*- (*UY*) directions, with the blue rollers denoting nodes with a fixed displacement UY or UX equal to 0 and the red arrows nodes with a predefined applied displacement which is greater or less than zero (depending on whether a tensile or compressive load is applied)

δl_y, with the former being defined by the applied strain ε_x, for loading in the *x*-direction. On the other hand, the internal angles of the simulated cell, γ (see Fig. 1), are fixed at 90° throughout deformation. This means that the only allowed changes in simulated cell dimensions are the lengths of the sides.

Extracting the Young's modulus, E_x, and Poisson's ratio, ν_{xy}, of this system is very straightforward. For the former, first the reaction forces in the *x* direction, RF_x, on all the nodes on the loaded edge (*Yb*) are summed up and divided by l_y to obtain the stress, σ_x, (assuming unit thickness) which is then divided by the applied strain, ε_x, to obtain the Young's modulus (see Eq. 1). For the latter, first, the displacement of one node on the unfixed transverse edge (*Xb*), *UY*, is divided by l_y to obtain the strain in the transverse direction, ε_y. This calculated parameter is then divided by $-\varepsilon_x$ to obtain the Poisson's ratio (see Eq. 2). The final equations based on the parameters obtained directly from the post-processing of the simulation (RF_x and *UY*) and initial and loading variables (l_y and ε_x) are shown in Eqs. 1 and 2.

$$E_x = \frac{\sum \left(RF_{x,Yb}\right)}{l_y} \frac{1}{\varepsilon_x} \tag{1}$$

$$V_{xy} = -\frac{UY}{l_y} \frac{1}{\varepsilon_x} \tag{2}$$

This approach has been used by many researchers in the literature to simulate a number of auxetic metamaterial systems, with the most prominent examples being rotating square systems [14, 22, 27, 28], anti-tetrachiral honeycombs [13, 14, 29] and re-entrant hexagonal honeycombs [12, 14, 20]. However, the validity of this method appears to hinge on the type of representative unit cell chosen. Figure 2 shows two sets of simulated cells which may be used to simulate a rotating square [30] (A) and re-entrant honeycomb [31–33] (B) system made up of (i) 1 × 1, (ii) 1 × 2 and (iii) 2 × 2 repeating units. Using ANSYS® Release 13.0 [34] FE software, each of these systems was modelled and simulated under uni-axial loading using the same boundary conditions shown in Fig. 1. The following parameters (see Fig. 2 A1(i), B1(i)) were used: the lengths of the rotating squares, $a = b = 1$, the angle between the squares, $\varphi = 60°$ and the amount of horizontal overlap between squares, $o = 0.1$ while for the re-entrant honeycomb, the lengths of the ribs, $l = 1$, $h = 1.5$, the angle of the inclined rib, $\theta = 30°$ and the thickness of the ribs, $t = 0.1$. In both cases, the joints were also rounded in order to avoid the use of sharp corners which could result in unrealistic stress distribution at the joint regions. Following mesh convergence testing, the re-entrant honeycombs were meshed using a uniform mesh size of $t/2$, while a smart sizing option was used for the rotating unit systems (with additional refinement at the joint regions) coupled with mesh mapping of the outer edges of the cell using a mesh size of $o/2$. A linear static analysis was used to find the mechanical properties of each system. The intrinsic material properties used were $\nu_{mat} = 0.3$ and $E_{mat} = 200$ GPa.

The resultant mechanical properties obtained from these simulations are shown in Fig. 3a. As one can observe, the Poisson's ratios and Young's moduli of the A1 and B1 simulations sets are consistent at values of ca. $\nu_{xy} = -0.96$, $E_x = 1135$ MPa and $\nu_{xy} = -0.97$, $E_x = 704$ MPa, respectively, regardless of the number of repeating units present in the simulated cell. However, in the case of sets A2 and B2, the mechanical properties of these systems vary significantly, indicating that the boundary conditions used are constraining the system and preventing it from deforming in its natural manner and thus are not suitable to model periodic boundary conditions.

This anomalous behaviour may be explained if one examines closely the deformation mechanism of these systems.

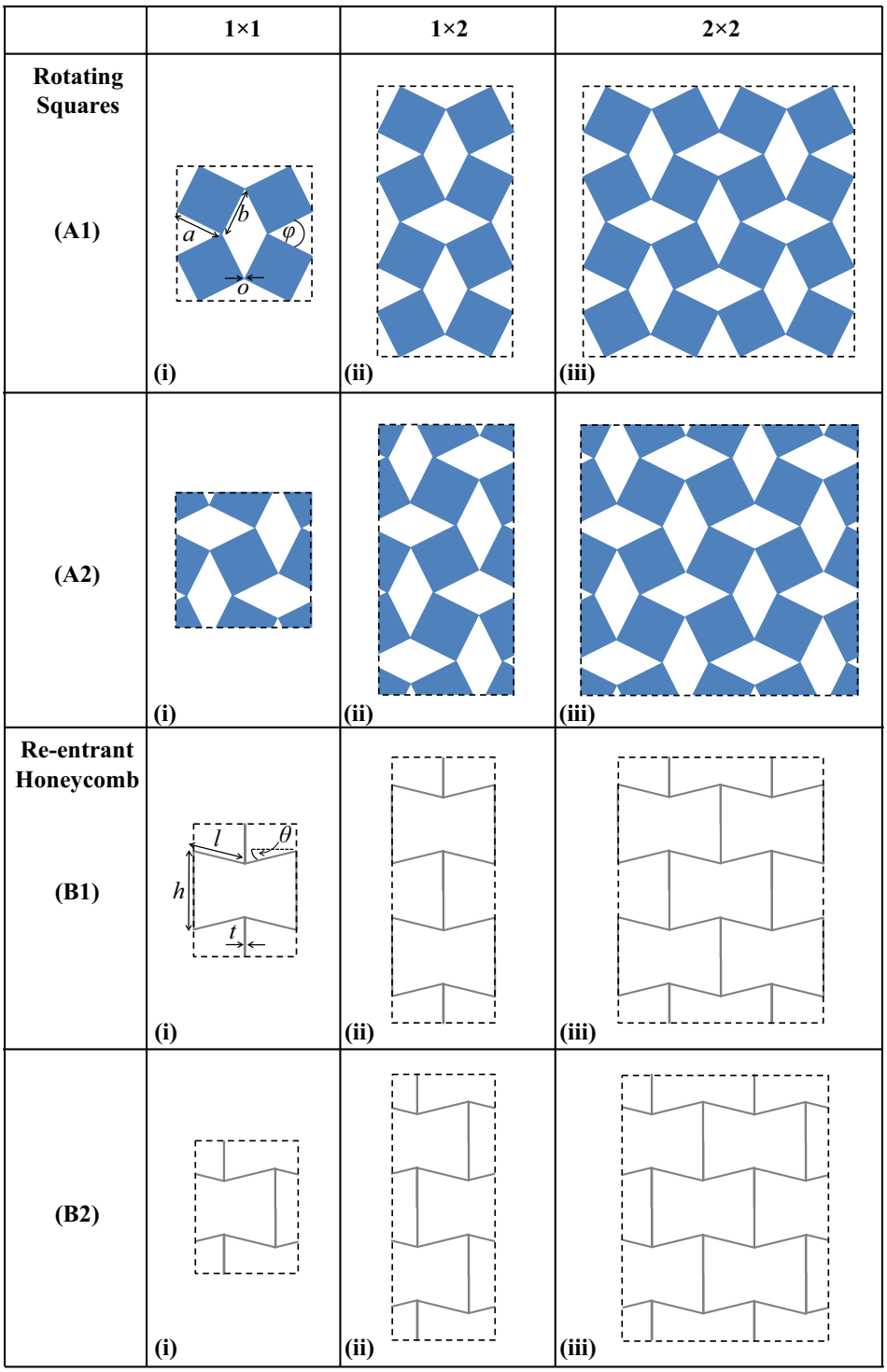

Fig. 2 Depictions of two sets of representative cells (1 and 2) of a rotating square system (**A**) and re-entrant honeycomb (**B**) system using (i) 1 × 1, (ii) 1 × 2 and (iii) 2 × 2 repeating unit cells

The rotating square system, as its name implies, deforms primarily through rotation of the square units (see Fig. 4), with each square pushing the neighbouring one to achieve an overall negative Poisson's ratio. As one can observe from Fig. 4a, in the case of the simulated cell shown in Fig. 2A1(i), the nodes at the boundaries of the cell (marked in blue) remain parallel to each other and the cell edges throughout deformation. On the other hand, in the case of the simulated cell shown in Fig. 4b, the boundary nodes on the same edge do not remain parallel to each other and the simulated cell edges during this form of deformation; hence the applied PBCs using strains and fixes are preventing the system from deforming in its natural manner resulting in an artificial constraint. This is clearly evident

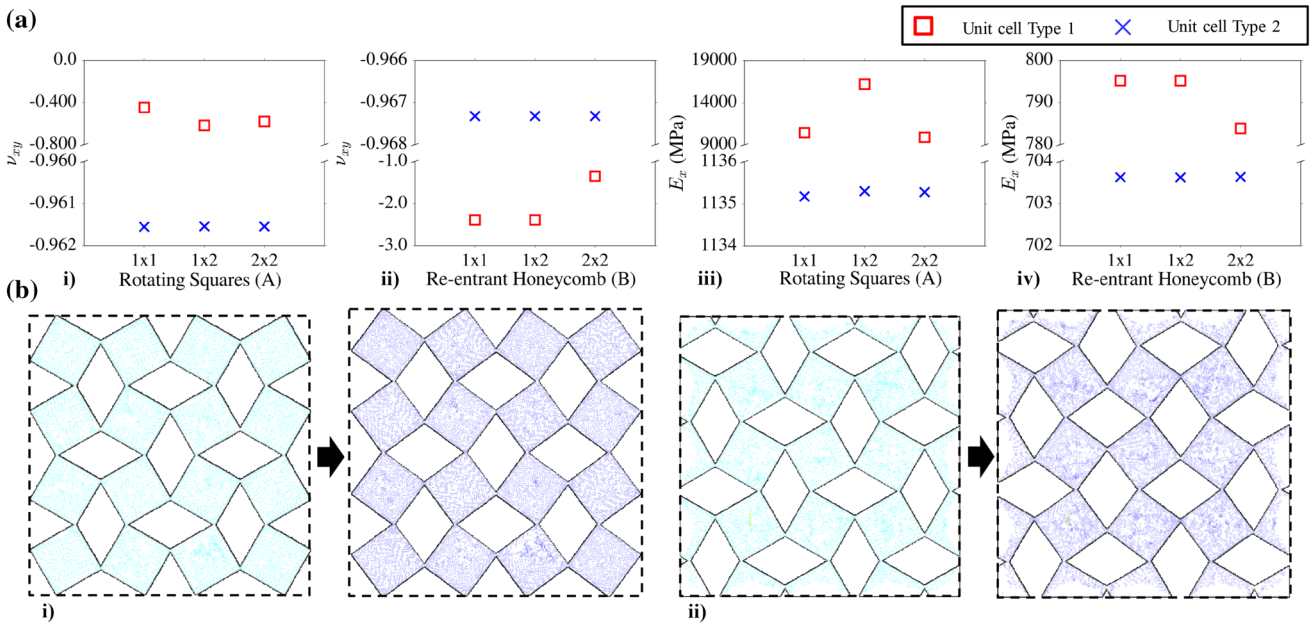

Fig. 3 **a** Plots showing the Poisson's ratios (i, ii) and Young's moduli (iii, iv) of the systems shown in Fig. 2 using Method 1 PBCs. **b** Diagrams showing the deformed and undeformed states of the rotating square systems shown in i) Fig. 2A1(iii) and ii) Fig. 2A2(iii)

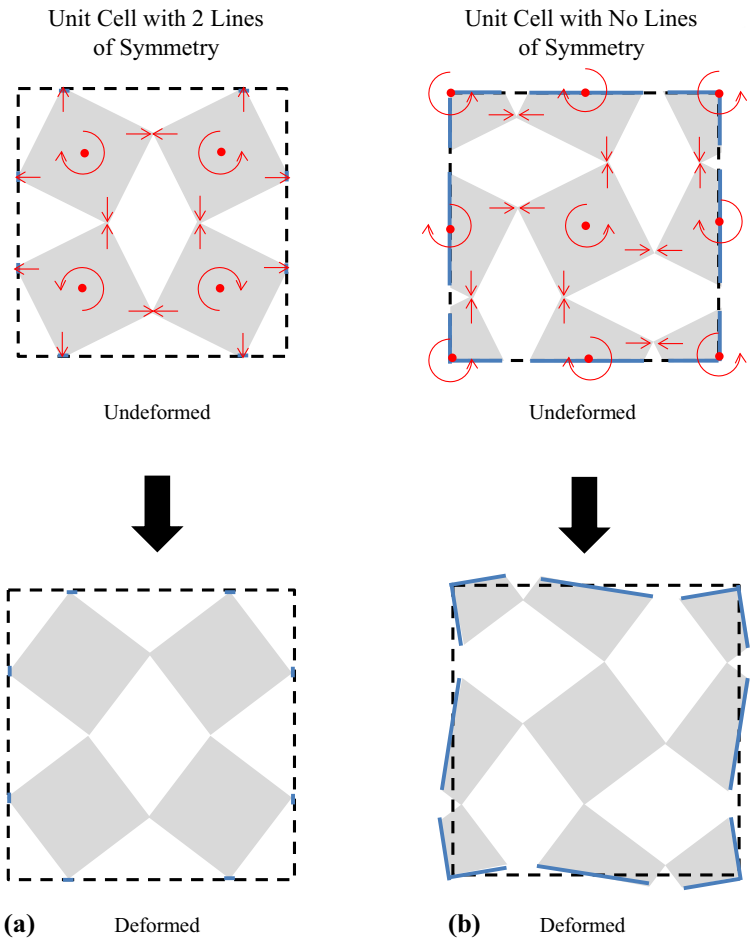

Fig. 4 Diagrams depicting the deformation of rotating square systems through the idealized rotating rigid unit mechanism. As one may observe while the first (**a**) representative unit cell retains its boundary shape throughout deformation, the other one (**b**) does not, hence rendering the PBCs used invalid for this type of unit cell

from Fig. 3b(i), where while the deformation of the system shown in Fig. 2A1(iii) is symmetric, i.e. all pores retain their rhombic shape during deformation, that of the corresponding system with the simulated cell shown in Fig. 2A2(iii) is far less symmetric with the pores near the boundary losing their rhombic shape to a greater extent than those in the central positions, indicating that rotation of squares on the boundaries is significantly more inhibited than that of those at the centre (see Fig. 3b(ii)).

To predict the suitability of this PBCs method to simulate on-axis loading of mechanical metamaterials, one must look at the symmetry of the representative unit cell geometry. The designs of the cells illustrated in Fig. 2A1 and B1 possess two lines of symmetry, with both lines being parallel to the on-axis loading directions. In addition, as one can observe from Fig. 3b, the deformation of these systems is also symmetric along the same lines of symmetry. On the other hand, the systems in Fig. 2A2 and B2 all lack this symmetry order, both in geometry and deformation mechanism. This proves that these PBCs are appropriate only to model unit cell geometries which possess these symmetry characteristics and are not suitable for cells which have an internal structure which lacks them. For this reason, these PBCs have been shown in previous works to accurately simulate systems such as anti-tetrachiral honeycombs [23, 29, 35] and Type I rotating rectangles [36], which can also possess the same symmetry order if modelled using the proper simulation cell, i.e. a cell which possesses the necessary symmetry requirements. We also predict that these PBCs are appropriate for investigating the on-axis mechanical properties of Type β rotating rhombi [37–40], Type Iβ parallelograms [39, 40], cases of specialized rotating triangle systems with two lines of symmetry [41], 4-Star re-entrant systems [42] and their corresponding fractal/hierarchical geometries [43–46].

The two cases investigated here highlight the main advantages and disadvantages of this PBCs method. Although in the two cases shown above it is possible to circumvent the symmetry problems by employing the appropriate unit cell geometry, in other cases such as hexachiral honeycombs [47] or generic rotating parallelograms [40], it is geometrically impossible to employ a rectangular unit cell which possesses the necessary symmetry requirements. Moreover, these PBCs are also unsuitable to simulate disordered or defective systems, since these involve the introduction of perturbations in the geometry which almost invariably result in a loss of symmetry. Thus, it is of essential importance to use an alternative PBCs technique which is suitable for all mechanical metamaterial geometries, regardless of the symmetry characteristics of the design in question.

2.3 Periodic boundary conditions applied through constraint equations (Method 2)

The alternative PBCs presented here are implemented through the use of constraint equations. Constraint equations are used to force the displacement of the nodes on one boundary onto the corresponding nodes on the opposite periodic boundary. This method does not enforce the edge nodes to retain their original alignment with adjacent nodes (similar to how particles are constrained to retain periodicity in molecular dynamics [48] and Mone Carlo simulations [49, 50]). The constraint equations, which are described by the displacement relationships derived by Suquet [51] require that, first, pairs of nodes are identified such that each node lies on a periodic boundary opposite each other occupying the same position along the respective boundary. This requirement implies that the number and position of nodes on opposing periodic boundaries are identical. Once the node pairs are identified, the periodic boundary conditions can be implemented by ensuring that the difference in displacement in the x and y directions is identical for all these node pairs [52] (see Fig. 5).

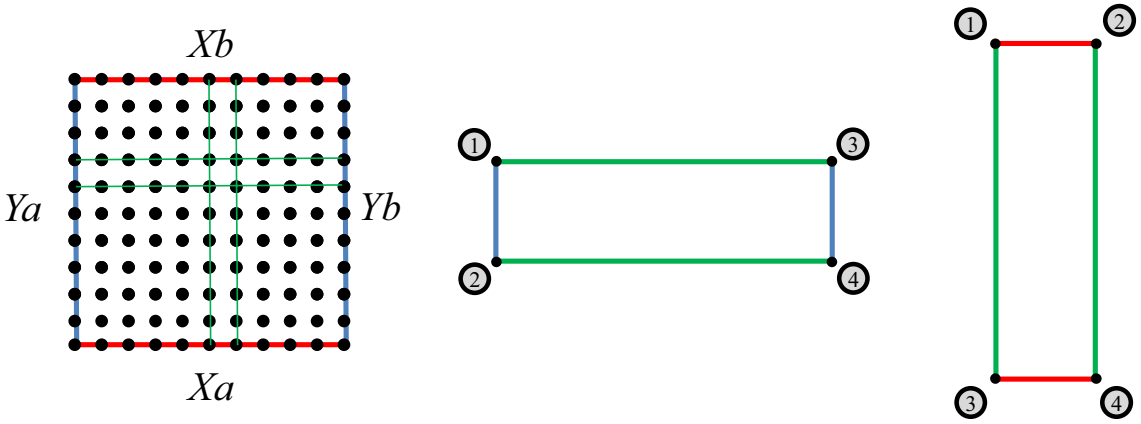

Fig. 5 Diagram showing how the edge nodes denoted by the blue line and those by the red lines are paired separately with each other

The constraint equations may be formulated in the following manner (Eqs. 3 and 4) for the displacements of every boundary node in the x- and y-directions:

$$UX1 - UX3 = UX2 - UX4 \tag{3}$$

$$UY1 - UY3 = UY2 - UY4 \tag{4}$$

where $UX1/UY1$ and $UX2/UY2$ denote the displacements of two nodes on the same edge and $UX3/UY3$ and $UX4/UY4$ signify the displacements of the two nodes directly opposite them on the other edge (see Fig. 5).

However, here it must be noted, that although the boundary conditions of the system have been defined, in order to simulate loading, the system must still be fixed from a point and loaded. The ideal way to fix a system in such a manner so as to not produce artificial constrains such as those identified for the PBCs in the previous section is to pin it from one point only. However, pinning the system from one point would still result in rigid body motion, which would make attaining a solution impossible. In order to get around this problem, the system is fixed from one point at the boundary ($UX = 0$ and $UY = 0$) and also fixed from the corresponding opposing edge node in the direction perpendicular to the line between these two nodes. Four examples of this are shown in Fig. 6. Although technically with this method the system is 'fixed' from two points, under the conditions imposed by periodicity, the edge nodes on opposing boundaries are for all ends and purposes of the simulation 'identical' and thus represent a single point in an infinite system. Furthermore, besides preventing rigid body motion and not imposing any additional constraints on the system, this also ensures that the system remains aligned with either the x- or y-axis during deformation. The final step is to apply a load on the system. Rather than using the direct application of strain through imposed displacements, the system is loaded through the application of a force on one set of nodes at the two opposing edges of the unit cell normal to the loading direction (see Fig. 6). The force is then distributed along the edges of the unit cell through the previously defined constraint equations in order to induce deformation of the unit cell. This is extremely important, since force loading, unlike strain loading, does not impose any constraints on the displacement of the nodes and thus, if need be, an edge node may actually move in the direction opposite to that of the applied force.

As one may observe from Fig. 6, Method 2 is not limited solely to rectangular unit cells, like Method 1, and may also be applied to parallelogramic unit cells. However, special care must be taken when a parallelogramic unit cell is used since this type of unit cell may only be

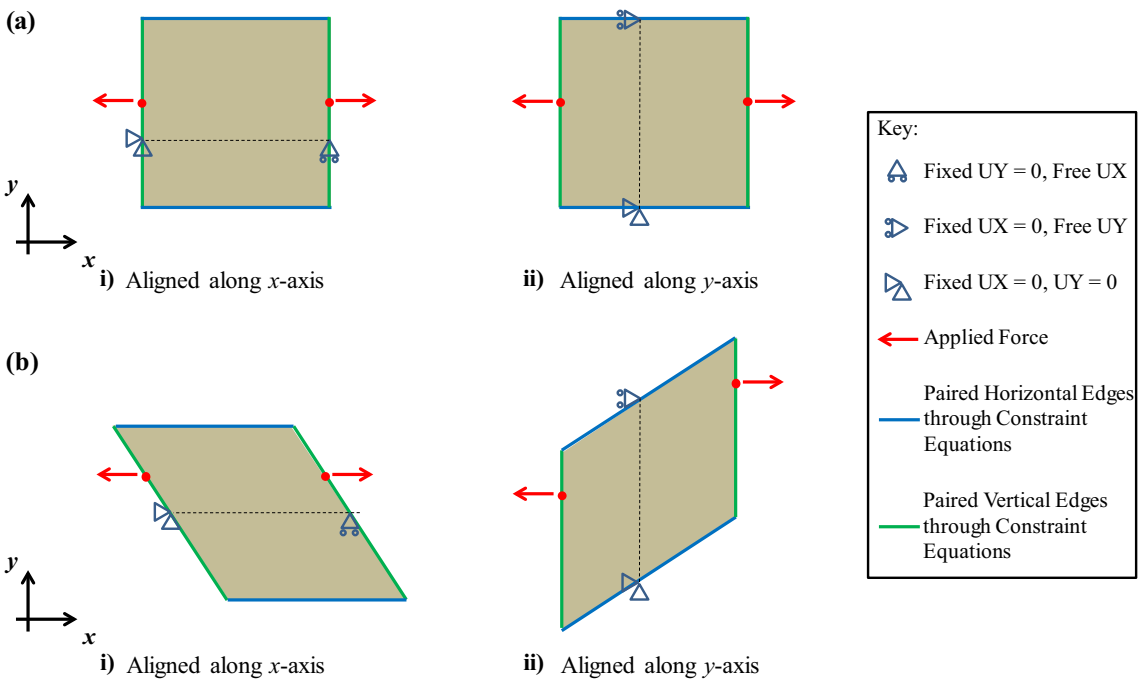

Fig. 6 Diagram showing the PBCs as applied for tensile loading of a **a** rectangular and **b** parallelogramic unit cell in the x-direction with the entire system aligned along the **i** x- and **ii** y-axis. Note that in the case of the system with the parallelogramic unit cell, a different unit cell must be used in order to align the geometry with the x- and y-axes since the system can only be aligned along the axis which is parallel to one set of sides of the unit cell. Also, note that it is immaterial on which point on the surface the force is applied, provided that it is applied on two corresponding boundary nodes in opposite directions

aligned with one axis. Therefore, if one wishes to align the system with the x-axis, then a unit cell which has one set of sides aligned with the x-axis must be chosen such as the one shown in Fig. 6b(i), while if the system is to be aligned with the y-axis, a unit cell such as the one shown in Fig. 6b(ii) must be used. Once the system is aligned with an axis it may be loaded in either the x- and y-directions in the same manner as a rectangular unit cell, i.e. by applying a force on the edge nodes. Here it is important to note that changing the unit cell does not mean rotating the unit cell to align it with a particular axis, but rather that a different representative unit cell is used to simulate the same geometry.

In this case, the calculation of the Poisson's ratio and Young's modulus is done differently since the known loading parameter is F_x, the force applied at the loading boundaries, rather than the strain, ε_x. The stress applied to the system, σ_x, can be calculated by dividing F_x by the length of this boundary, l_y (assuming unit thickness). In order to calculate ε_x and ε_y, the displacements at all boundaries have to be considered. Due to the applied constraint equations (see Eqs. 3 and 4), the total displacement between each paired set of opposing boundary nodes is identical. Therefore, the resultant displacement following deformation may be extracted from one pair of nodes each on the vertical (UX_{Ya} and UX_{Yb}) and horizontal (UY_{Xa} and UY_{Xb}) boundaries. The Poisson's ratio and Young's modulus may be calculated as:

$$E_x = \frac{F_x}{l_y}\frac{l_x}{\left(UX_{Yb} - UX_{Ya}\right)} \tag{5}$$

$$V_{xy} = \frac{\left(UY_{Xb} - UY_{Xa}\right)}{l_y}\frac{l_x}{\left(UX_{Yb} - UX_{Ya}\right)} \tag{6}$$

In order to validate this PBCs method, a similar approach to that adopted in the previous section was employed. The systems shown in Fig. 2 were all simulated using the same parameters as in the previous chapter, with the exception that the PBCs described in Fig. 6 were used. The systems were aligned along the y-axis (as in Fig. 6a(ii)) and loaded in the x-direction.

The mechanical properties obtained from these simulations are plotted in Fig. 7a below. As one may observe, all unit cells of the rotating square and re-entrant system have almost exactly the same mechanical properties regardless of the number of repeating units in the simulated cell or type used. In fact, as shown in Fig. 7b, the deformation profile of the systems shown in Fig. 2A1(iii) and A2(iii) are almost identical to each other and those shown in Fig. 4 (note that the pores retain their rhombic shape in both cases).

These results highlight the advantages of this PBCs method over the previous one employed to model the same geometries. Since this method does not impose any fixed displacement constraints on the boundary nodes, there are no symmetry requirements for the internal geometry of the unit cell for it to function properly. In addition, these PBCs

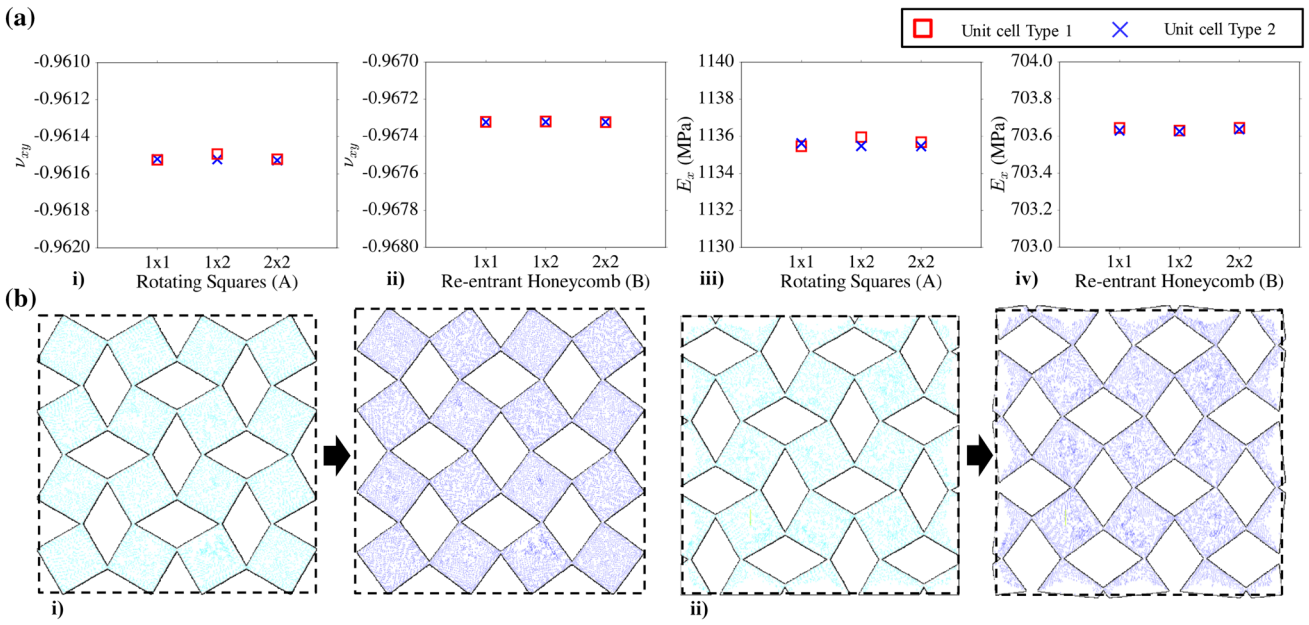

Fig. 7 **a** Plots showing the (i) Poisson's ratios and (ii) Young's moduli of the systems shown in Fig. 2 using Method 2 PBCs. **b** Diagrams showing the deformed and undeformed states of the rotating square systems shown in (i) Fig. 2A1(iii) and (ii) Fig. 2A2(iii). Note that all the results are almost exactly identical regardless of unit cell size or type of repeating unit

can also be implemented to study systems with parallelogramic unit cells such as the schematics shown in Fig. 6b as well as geometries which possess non-zero shear coupling coefficients. The internal angle of the unit cell, γ, is not fixed through this method, and thus shearing deformation is permissible through this approach.

In order to check the validity of this approach on more complex geometries, we implemented these PBCs on two

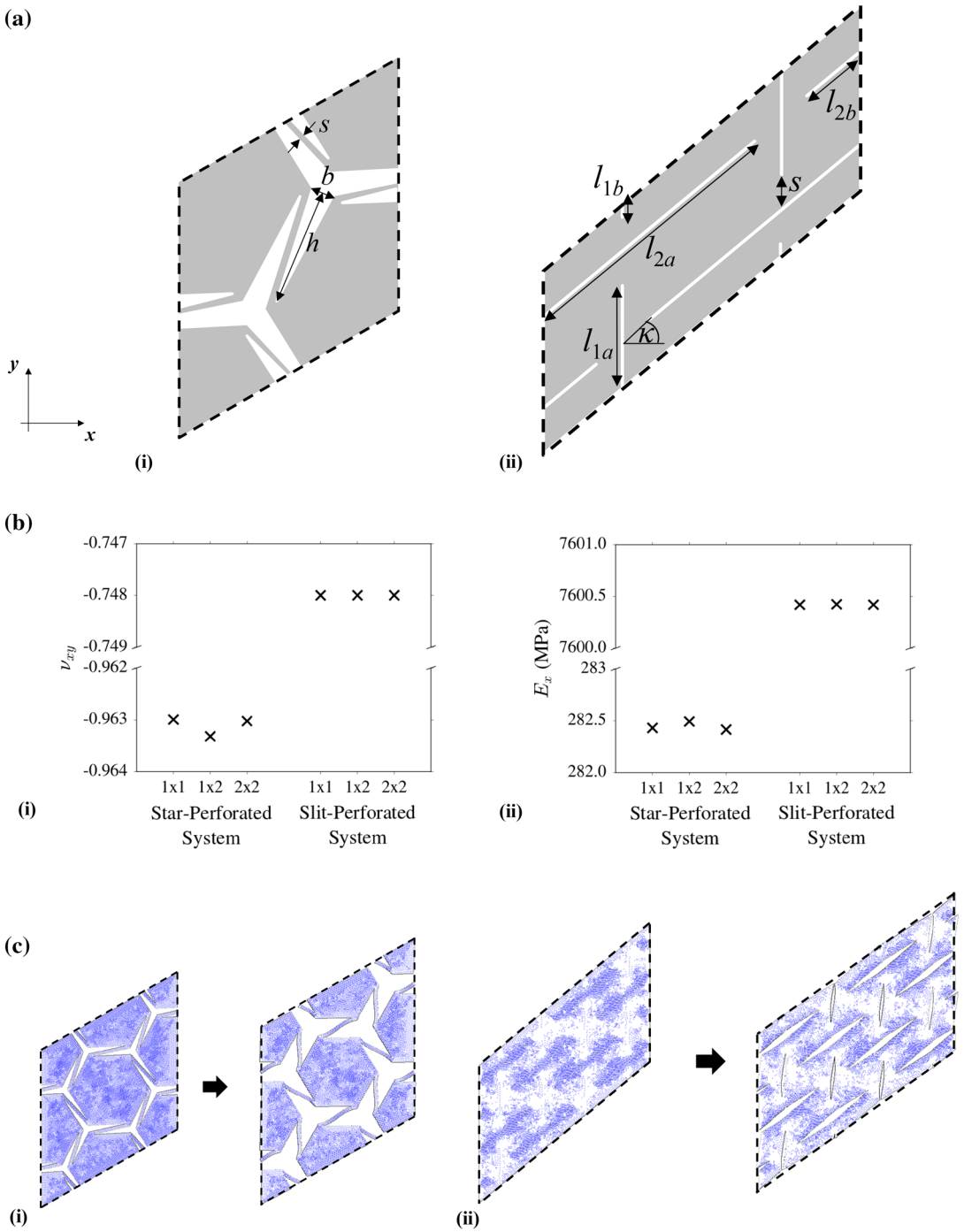

Fig. 8 **a** A depiction of a 1×1 unit cell of a (i) three-pointed star perforated system and (ii) an alternating straight line slit perforated system indicating the parameters used to define the metamaterial geometries. **b** Plots showing the (i) Poisson's ratios and (ii) Young's Moduli obtained for loading these systems in the x-direction. **c** Figures showing the deformed and undeformed state of the 2×2 systems simulated here. Note that displacement scaling was used to generate these diagrams since a linear geometric solution was used to obtain the mechanical properties

examples of auxetic mechanical metamaterial geometries recently proposed by the same authors; namely the (a) three-pointed star perforated system [15] and (b) slit perforated system [14] (see Fig. 8a). Both of these designs have geometric characteristics which make them particularly challenging to simulate. As shown in Fig. 8, the former system has a 'fragmented' representative geometry while the latter is based on the rotating parallelogram mechanism [40], which is known to undergo shear deformations during uniaxial loading. In analogy with the approach employed previously, both these systems were modelled as 1×1, 1×2 and 2×2 simulation cells aligned along the y-axis and loaded in the x-direction. For the star perforated system, the parameters (see Fig. 8a(i)) were set at $b=1$, $h=6$ and $s=0.4$ while for the slit perforated system (see Fig. 8a(ii)) $l_1=1$, $l_2=2$, $\kappa=40°$, s = 0.3 and $t=0.01$ were used.

As shown in Fig. 8b, both systems were successfully simulated for loading using these PBCs with each unit cell giving the same resultant mechanical properties regardless of the number of repeating units inside it. In the case of the three-pointed star perforated system, although the system may appear to be made up of three disjointed fragments, in reality these pieces are connected to each other through the constraint equations at the boundary nodes and thus rigid body motion is not observed. For the slit perforated system, as one may observe from Fig. 8c(ii), the internal angle of the unit cell, γ, changed during deformation, indicating that the system has successfully undergone shear deformation. All this indicates that this PBCs method is also suitable to investigate complex systems with 'fragmented' parallelogramic unit cells, as well as systems with the potential to undergo shear deformation. This includes mechanisms and geometries such as rotating triangles [36, 53–57], rotating parallelograms [39, 40], chiral honeycombs such as hexachiral, tetrachiral, metachiral and trichiral systems [23, 47, 58–64] and other geometries [65–69] which do not meet the symmetry requirements for the Method 1 PBCs.

Here it should be noted that although force loading was implemented in the Method 2 examples provided here, in certain cases direct displacement loading can also be applied. In cases where the loading is in the same direction as the axis along which the system is aligned, one has to simply apply a fixed displacement on the aligned node only, the rest will follow due to the imposed constraint equations. The reaction force required to calculate the force may be obtained directly from the node upon which the force is applied. However, in cases where loading in any of the on-axis directions other than that of the desired alignment of the unit cell is required, care must be taken to ensure that additional artificial constraints are not imposed on the system when applying a fixed displacement since this will require the imposition of a deformation constraint on an additional point of the periodic system besides the one used to maintain the unit cell alignment. Therefore, if one desires certainty that the implemented methodology is correct in such cases, it is recommended to use force loading rather than displacement loading.

3 Discussion

In the previous section, two PBCs methods which may be used to simulate 2D mechanical metamaterial geometries were presented. At this point, it is important to reiterate that both Methods 1 and 2 are strictly speaking computationally and mathematically correct for any geometry; in the sense that both methods produce a system which deforms in a periodic manner. However, as shown in the previous sections, in order to simulate the deformation of a realistic system without artificial constraints imposed as a result of the PBCs used, certain conditions and criteria must be met. The main differences between these two methods are summarized in Table 1 below.

It is clear that the second method presents a number of obvious advantages over the first, with the most important being that it is completely generalized and may be used to simulate any 2D geometry. Besides being ideal to model complex geometries, this also makes it suitable to investigate disordered systems. For the study of disordered systems, typically, a unit cell made up of a large number of repeating units is used. Disorder is then introduced within the system through the use of geometric perturbations which disrupt the symmetry of the system. Although the notion of using PBCs to study disordered systems may sound paradoxical at first glance, since periodic 'disorder' is essentially order with a lower degree of symmetry than periodic order, it is well known that boundary or edge effects have a considerable influence on the deformation of the system. Thus, if one wishes to completely isolate the effect of disorder from

Table 1 Table highlighting the main differences between the two PBCs methods presented in this work

	PBCs Method 1	PBCs Method 2
Unit cell shape	Rectangular only	Rectangular or parallelogramic
Symmetry requirements	Two lines of symmetry aligned with the x- and y-axis	None
Boundary mesh mapping	Not required	Essential
Loading type	Displacement or force loading may be used	Force loading
'Fragmented' unit cell	Not allowed	Allowed
Shear deformation	Not allowed	Allowed

that of the edge effect, the PBCs method is the only possible way to do this. This approach has been used by a number of researchers in literature [70–76] to investigate the intrinsic effect of disorder and defects on the mechanical properties of mechanical metamaterials and the PBCs discussed in Method 2 would be ideal for this purpose since they are symmetry independent.

However, the PBCs Method 2 presented here is also relatively more difficult to implement than Method 1. The validity of Method 2 depends completely on the condition that all paired nodes on opposing edges correspond exactly with each other with respect to the initial position. This means that the mesh at the boundaries of the unit cell must be mapped in order to ensure that the correct nodal positions are achieved and thus one cannot simply employ a uniform smart sizing or similar options which are typically found in commercial FE software to mesh these systems. On the other hand, this is not a problem in Method 1. Although having an unequal number of nodes at the boundaries is not considered ideal (due to the introduction of minute asymmetry within the system), having slightly different mesh geometries at the boundaries does not normally have a significant adverse effect on the deformation of the system when using the strains and fixes method to employ PBCs. This means that for Method 2 to be used, a more thorough mesh convergence testing must be conducted first to ensure the validity of the simulations than in the case of Method 1.

The methodologies presented here have only been applied to 2D geometries. However, the same approach may also be extended to include 3D systems. For Method 1, the PBCs may be implemented as shown in Fig. 9 for loading in the x-direction. Again, this method suffers from the same drawbacks as its 2D variant: shearing deformations are not allowed; a cuboidal, non-'fragmented' internal unit cell geometry must be used; and the system must now have three planes of symmetry aligned along each of the three main Cartesian planes, xy, yz and xz in order for the PBCs to impose no additional constraints on the system.

In the case of Method 2, the same methodology can also be applied. Constraint equations are used to pair opposing nodes together on each face of the unit cell boundary using the relationships defined in Eqs. 3 and 4 as well as the additional equation defined in Eq. 7 below, which enforces periodicity in displacements in the z-direction, UZ, as well.

$$UZ1 - UZ3 = UZ2 - UZ4 \tag{7}$$

In this case, rather than along an axis, the unit cell is aligned relative to a plane instead. Thus, as shown in Fig. 10 below, there are three options when aligning the unit cell, the xy-, xz- or yz-plane, which is one more than that available for the 2D system (either along x- or y-axis). Similarly to the 2D method, the unit cell is also allowed to undergo shearing deformations in any of the three planes and a parallelepiped and/or 'fragmented' unit cell is permitted. Obviously, when using a parallelepiped unit cell, the same limitations and conditions indicated for choosing the appropriate unit cell based on the desired alignment indicated for 2D systems hold as well. The unit cell surfaces must also be meshed using mapped elements, in this case with area, rather than line mapping.

To summarize, both methods investigated here have been shown to be valid and suitable for simulating on-axis loading of 2D and 3D mechanical metamaterials, provided that the appropriate conditions are met. In the case of Method 1, although it is easier and computationally more efficient to implement than Method 2, the symmetry requirements

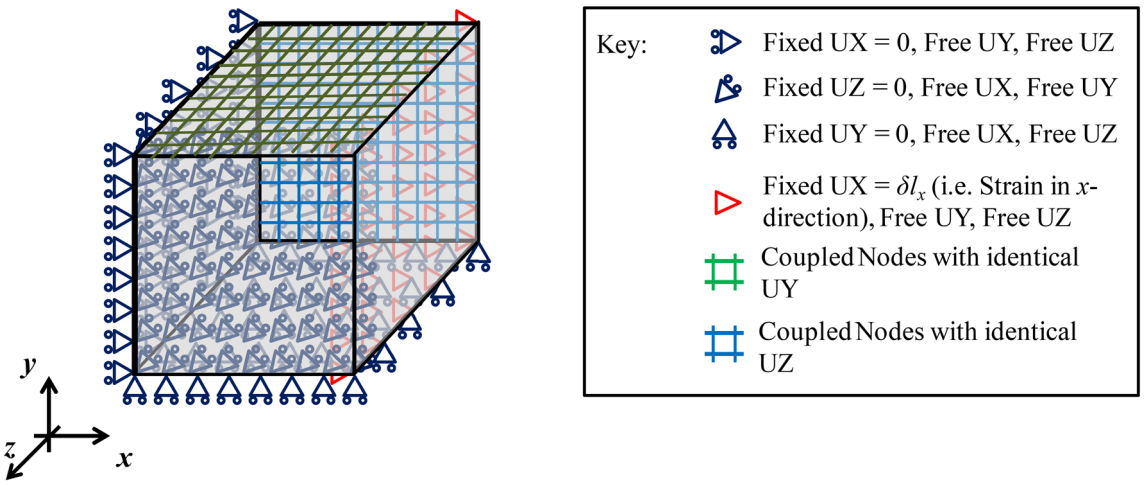

Fig. 9 Schematic showing how the PBCs used in Method 1 may be implemented in a cuboidal unit cell. One unit cell side boundary aligned with each Cartesian axis is fixed in the direction normal to its plane, the side upon which the strain is applied is given a fixed displacement in the x-direction, UX, and the nodes on the remain two faces of the unit cell are coupled to retain their planar shape

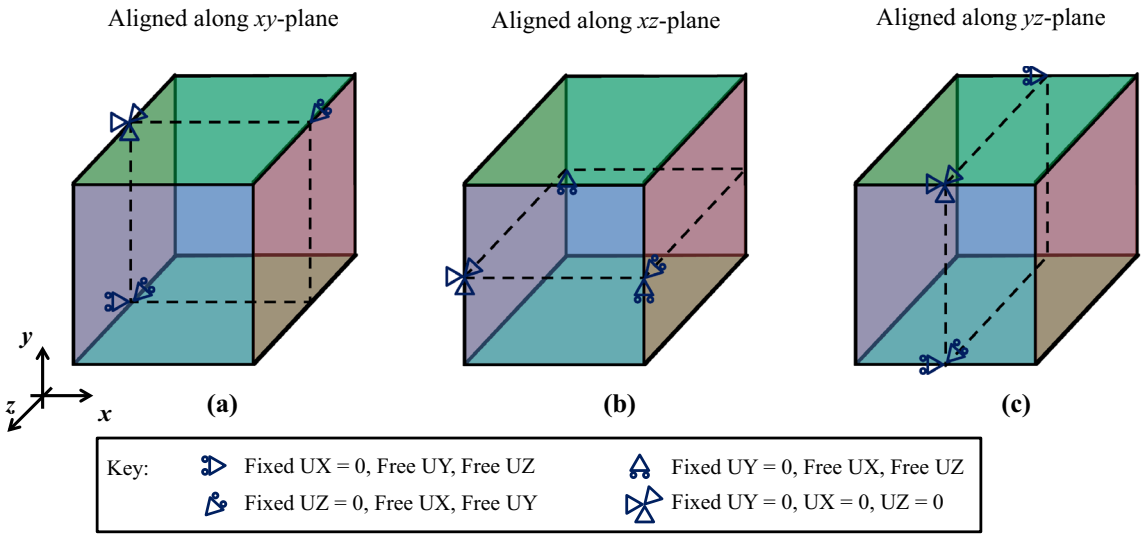

Fig. 10 Schematic showing how the PBCs used in Method 2 may be implemented in a cuboidal unit cell aligned along the **a** *xy*-, **b** *xz*- and **c** *yz*-plane. The coloured faces of the unit cell indicated surfaces where the nodes are paired using constraint equations (blue, red and green), while the black dotted line denotes the plane along which the unit cell is aligned

and deformation mechanism within the unit cell indicate that this method should only be applied to systems where some degree of prior knowledge of deformation modes and behaviour is available. On the other hand, Method 2, while being more computationally demanding and complex to implement, it was shown to be extremely more versatile and can be employed to study any system with a quadratic unit cell, regardless of symmetry or internal angle of the cell. This makes this method particularly suitable to study novel mechanical metamaterial geometries and disordered systems.

At this point, it is important to emphasize that the methods consider only the simulation of on-axis tensile and compressive loading in the *x*- and *y*-directions (and *z* in the case of 3D systems) of periodic systems. Obviously, the periodic boundary conditions stipulated in Eqs. 3, 4 and 7 would still be valid for maintaining periodicity throughout deformation in cases of pure shear deformation and off-axis loading, however, different loading and fixing conditions are required in order to correctly implement and simulate these conditions. Moreover, it should be highlighted that although both Method 1 and 2 were validated on systems which were simulated under linear conditions, the same assumptions and methods are also valid for conducting simulations under high strain, nonlinear conditions. Finally, before concluding, it is important to highlight that using PBCs to investigate the mechanical properties and deformation behaviour of a system should always be considered to be merely the first step in the analysis of a novel metamaterial structure. This is due to the fact that, although a system simulated under PBCs provides significant insights into the deformation behaviour of the structure, it gives no information about the influence of boundary effects on the metamaterial geometry in question and other derived characteristics of this factor such as the propagation of deformation throughout a finite system made up of multiple unit cells. As shown in a recent study on a range of finite perforated metamaterial geometries [77], each metamaterial system shows a distinct deformation propagation profile. These profiles and other boundary effects cannot be investigated through the use of infinite systems, and thus, in addition to the preliminary, less computationally intensive FE simulations using PBCs on a single repeating unit, further FE analysis on large finite systems and experimental samples containing multiple RVEs are still required in order to obtain a complete picture of the actual deformation and load response of a real-life metamaterial system.

4 Conclusion

In this work, we have examined a commonly known PBCs method (Method 1) and presented another alternative (Method 2), which may be used to simulate on-axis loading of complex mechanical metamaterial geometries using PBCs. The first method is relatively easy to implement but is only suitable for a limited number of geometries and unit cell types which meet a restrictive set of criteria defined in this paper. On the other hand, the second method is more generalized and has no symmetry limitations meaning that it may be used for any mechanical metamaterial geometry or otherwise, as well as for the study of disordered systems or systems with defects. Both these PBCs methods may also be applied to 3D systems. It is envisaged that the work presented here will be of great importance to materials

scientists and structural engineers, particularly those whose work is centered on the development and study of mechanical metamaterials. Defining periodicity and applying the correct loading conditions is typically one of the most difficult steps encountered when simulating systems with complex topologies, particularly in the case of novel systems, and it is hoped that the insights and methods presented in this work will considerably aid researchers at this stage of their research and advance their endeavors in discovering and studying new materials and systems.

Acknowledgements K.K.D. acknowledges the financial support from the program of the Polish Minister of Science and Higher Education under the name "Regional Initiative of Excellence" in 2019–2022, project no. 003/RID/2018/19, funding amount 11 936 596.10 PLN.

References

1. Evans KE, Nkansah MA, Hutchinson J, Rogers SC (1991) Molecular network design. Nature 353:124
2. Baughman RH, Shacklette JM, Zakhidov AA, Stafstrom S (1998) Negative Poisson's ratios as a common feature of cubic metals. Nature 392:362–365
3. Lakes R (1987) Foam structures with a negative Poisson's ratio. Science 235:1038–1040. https://doi.org/10.1126/science.235.4792.1038
4. Wojciechowski KW (1989) Two-dimensional isotropic system with a negative poisson ratio. Phys Lett A 137:60–64. https://doi.org/10.1016/0375-9601(89)90971-7
5. Sigmund O (1995) Tailoring materials with prescribed elastic properties. Mech Mater 20:351–368
6. Ishibashi Y, Iwata M (2000) A microscopic model of a negative Poisson's ratio in some crystals. J Phys Soc Jpn 69:2702–2703. https://doi.org/10.1143/JPSJ.69.2702
7. Dudek MR, Grabiec B, Wojciechowski KW (2007) Molecular dynamics simulations of auxetic ferrogel. Rev Adv Mater Sci 14:167–173
8. Lakes RS, Lee T, Bersie A, Wang YC (2001) Extreme damping in composite materials with negative-stiffness inclusions. Nature 410:565–567
9. Baughman RH, Stafstrom S, Cui C, Dantas SO (1998) Materials with negative compressibilities in one or more dimensions. Science 279:1522–1524. https://doi.org/10.1126/science.279.5356.1522
10. Nicolaou ZG, Motter AE (2012) Mechanical metamaterials with negative compressibility transitions. Nat Mater 11:608–613
11. Lakes R, Wojciechowski KW (2008) Negative compressibility, negative Poisson's ratio, and stability. Phys Status Solidi Basic Res 245:545–551. https://doi.org/10.1002/pssb.200777708
12. Mizzi L, Attard D, Casha A, Grima JN, Gatt R (2014) On the suitability of hexagonal honeycombs as stent geometries. Phys Status Solidi B 251:328–337. https://doi.org/10.1002/pssb.201384255
13. Gatt R, Attard D, Farrugia PS, Azzopardi KM, Mizzi L, Brincat JP et al (2013) A realistic generic model for anti-tetrachiral systems. Phys Status Solidi B 250:2012–2019. https://doi.org/10.1002/pssb.201384246
14. Mizzi L, Azzopardi KM, Attard D, Grima JN, Gatt R (2015) Auxetic metamaterials exhibiting giant negative Poisson's ratios. Phys Status Solidi Rapid Res Lett 9:425–430. https://doi.org/10.1002/pssr.201510178
15. Mizzi L, Mahdi EM, Titov K, Gatt R, Attard D, Evans KE et al (2018) Mechanical metamaterials with star-shaped pores exhibiting negative and zero Poisson's ratio. Mater Des 146:28–37. https://doi.org/10.1016/j.matdes.2018.02.051
16. Taylor M, Francesconi L, Gerendás M, Shanian A, Carson C, Bertoldi K (2014) Low porosity metallic periodic structures with negative Poisson's ratio. Adv Mater 26:2365–2370
17. Shan S, Kang SH, Zhao Z, Fang L (2015) Design of planar isotropic negative Poisson' s ratio structures. Extrem Mech Lett 4:96–102. https://doi.org/10.1016/j.eml.2015.05.002
18. Hassan MR, Scarpa F, Ruzzene M, Mohammed NA (2008) Smart shape memory alloy chiral honeycomb. Mater Sci Eng A 481–482:654–657. https://doi.org/10.1016/j.msea.2006.10.219
19. Carta G, Brun M, Baldi A (2016) Design of a porous material with isotropic negative Poisson's ratio. Mech Mater 97:67–75. https://doi.org/10.1016/j.mechmat.2016.02.012
20. Bezazi A, Scarpa F, Remillat C (2005) A novel centresymmetric honeycomb composite structure. Compos Struct 71:356–364. https://doi.org/10.1016/j.compstruct.2005.09.035
21. Shen J, Zhou S, Huang X, Xie YM (2014) Simple cubic three-dimensional auxetic metamaterials. Phys Status Solidi B 251:1–8. https://doi.org/10.1002/pssb.201451304
22. Jopek H, Strek T (2015) Thermal and structural dependence of auxetic properties of composite materials. Phys Status Solidi B 252:1551–1558. https://doi.org/10.1002/pssb.201552192
23. Alderson A, Alderson KL, Attard D, Evans KE, Gatt R, Grima JN et al (2010) Elastic constants of 3-, 4- and 6-connected chiral and anti-chiral honeycombs subject to uniaxial in-plane loading. Compos Sci Technol 70:1042–1048. https://doi.org/10.1016/j.compscitech.2009.07.009
24. Xia Z, Zhang Y, Ellyin F (2003) A unified periodical boundary conditions for representative volume elements of composites and applications. Int J Solids Struct 40:1907–1921. https://doi.org/10.1016/S0020-7683(03)00024-6
25. Xia Z, Zhou C, Yong Q, Wang X (2006) On selection of repeated unit cell model and application of unified periodic boundary conditions in micro-mechanical analysis of composites. Int J Solids Struct 43:266–278. https://doi.org/10.1016/j.ijsolstr.2005.03.055
26. Gao L, Wang C, Liu Z, Zhuang Z (2017) Theoretical aspects of selecting repeated unit cell model in micromechanical analysis using displacement-based finite element method. Chin J Aeronaut 30:1417–1426. https://doi.org/10.1016/j.cja.2017.05.010
27. Mizzi L, Gatt R, Grima JN (2015) Non-porous grooved single-material auxetics. Phys Status Solidi B 252:1559–1564. https://doi.org/10.1002/pssb.201552218
28. Poźniak AA, Wojciechowski KW, Grima JN, Mizzi L (2016) Planar auxeticity from elliptic inclusions. Compos Part B Eng 94:379–388. https://doi.org/10.1016/j.compositesb.2016.03.003
29. Gatt R, Brincat JP, Azzopardi KM, Mizzi L, Grima JN (2015) On the effect of the mode of connection between the node and the ligaments in anti-tetrachiral systems. Adv Eng Mater 17:189–198. https://doi.org/10.1002/adem.201400120
30. Grima JN, Evans KE (2000) Auxetic behavior from rotating squares. J Mater Sci Lett 19:1563–1565
31. Gibson LJ, Ashby MF, Schajer GS, Robertson CI (1982) The mechanics of two dimensional cellular materials. Proc R Soc A Math Phys Eng Sci 382:25–42
32. Abd El-Sayed FK, Jones R, Burgess IW (1979) A theoretical approach to the deformation of honeycomb based composite materials. Composites 1979:209–214
33. Masters IG, Evans KE (1996) Models for the elastic deformation of honeycombs. Compos Struct 35:403–422
34. ANSYS® Academic Research Mechanical, Release 13.0 (2013)
35. Sigmund O, Torquato S (1999) Design of smart composite materials using topology optimization. Smart Mater Struct 8:365–379. https://doi.org/10.1088/0964-1726/8/3/308

36. Grima BJN, Gatt R (2010) Perforated sheets exhibiting negative Poisson's ratios. Adv Eng Mater 2010:460–464. https://doi.org/10.1002/adem.201000005
37. Grima JN, Alderson A, Evans KE (2004) Negative Poisson's ratios from rotating rectangles. Comput Methods Sci Technol 10:137–145
38. Attard D, Grima JN (2008) Auxetic behaviour from rotating rhombi. Phys Status Solidi 245:2395–2404. https://doi.org/10.1002/pssb.200880269
39. Grima JN, Farrugia P-S, Gatt R, Attard D (2008) On the auxetic properties of rotating rhombi and parallelograms: a preliminary investigation. Phys Status Solidi 245:521–529
40. Attard D, Manicaro E, Grima JN (2009) On rotating rigid parallelograms and their potential for exhibiting auxetic behaviour. Phys Status Solidi B 2044:2033–2044. https://doi.org/10.1002/pssb.200982034
41. Dudek KK, Attard D, Caruana-Gauci R, Wojciechowski KW, Grima JN (2016) Unimode metamaterials exhibiting negative linear compressibility and negative thermal expansion. Smart Mater Struct 25:025009
42. Grima JN, Gatt R, Alderson A, Evans KE (2005) On the potential of connected stars as auxetic systems. Mol Simul 13:923–934
43. Tang Y, Lin G, Han L, Qiu S, Yang S, Yin J (2015) Design of hierarchically cut hinges for highly stretchable and reconfi gurable metamaterials with enhanced strength. Adv Mater 2015:1–10. https://doi.org/10.1002/adma.201502559
44. Cho Y, Shin J, Costa A, Ann T, Kunin V, Li J et al (2014) Engineering the shape and structure of materials by fractal cut. Proc Natl Acad Sci 111:17390–17395. https://doi.org/10.1073/pnas.1417276111
45. Gatt R, Mizzi L, Azzopardi JI, Azzopardi KM, Attard D, Casha A et al (2015) Hierarchical auxetic mechanical metamaterials. Sci Rep 5:1–6. https://doi.org/10.1038/srep08395
46. Dudek KK, Gatt R, Mizzi L, Dudek MR, Attard D, Evans KE et al (2017) On the dynamics and control of mechanical properties of hierarchical rotating rigid unit auxetics. Sci Rep 7:65–69. https://doi.org/10.1038/srep46529
47. Prall D, Lakes RS (1997) Properties of a chiral honeycomb with a Poisson's ratio of − 1. Int J Mech Sci 39:305–314
48. Parrinello M, Rahman A (1980) Crystal structure and pair potentials: a molecular-dynamics study. Phys Rev Lett 45:1196–1199
49. Wojciechowski KW, Branka A, Parrinello M (1984) Monte Carlo study of the phase diagram of a two dimensional system of hard cyclic hexamers. Mol Phys 53:1541–1545
50. Wojciechowski KW (1987) Constant thermodynamic tension Monte Carlo studies of elastic properties of a two-dimensional system of hard cyclic hexamers. Mol Phys 61:1247–1258
51. Suquet PM (1987) Homogenization techniques for composite media. Springer, Berlin
52. Miehe C, Schröder J, Schotte J (1999) Computational homogenization analysis in finite plasticity simulation of texture development in polycrystalline materials. Comput Methods Appl Mech Eng 171:387–418. https://doi.org/10.1016/S0045-7825(98)00218-7
53. Grima JN, Evans KE (2006) Auxetic behaviour from rotating triangles. J Mater Sci 41:3193–3196
54. Grima JN, Farrugia P-S, Gatt R, Zammit V (2006) Connected triangles exhibiting negative Poisson's ratios and negative thermal expansion. J Phys Soc Jpn 76:025001
55. Kunin V, Yang S, Cho Y, Deymier P, Srolovitz DJ (2015) Static and dynamic elastic properties of fractal-cut materials. Extrem Mech Lett. https://doi.org/10.1016/j.eml.2015.12.003
56. Zhou XQ, Zhang L, Yang L (2017) Negative linear compressibility of generic rotating rigid triangles. Chin Phys B 26:126201
57. Lim TC (2017) Analogies across auxetic models based on deformation mechanism. Phys Status Solidi Rapid Res Lett 11:1600440
58. Alderson A, Alderson KL, Chirima G, Ravirala N, Zied KM (2010) The in-plane linear elastic constants and out-of-plane bending of 3-coordinated ligament and cylinder-ligament honeycombs. Compos Sci Technol 70:1034–1041. https://doi.org/10.1016/j.compscitech.2009.07.010
59. Shim J, Perdigou C, Chen ER, Bertoldi K, Reis PM (2012) Buckling-induced encapsulation of structured elastic shells under pressure. Proc Natl Acad Sci 2012:1–6. https://doi.org/10.1073/pnas.1115674109
60. Bacigalupo A, Gambarotta L (2014) Homogenization of periodic hexa- and tetrachiral cellular solids. Compos Struct 116:461–476. https://doi.org/10.1016/j.compstruct.2014.05.033
61. Ha CS, Hestekin E, Li J, Plesha ME, Lakes RS (2015) Controllable thermal expansion of large magnitude in chiral negative Poisson's ratio lattices. Phys Status Solidi B 1434:1431–1434. https://doi.org/10.1002/pssb.201552158
62. Bettini P, Airoldi A, Sala G, Di Landro L, Ruzzene M, Spadoni A (2010) Composite chiral structures for morphing airfoils: numerical analyses and development of a manufacturing process. Compos Part B Eng 41:133–147. https://doi.org/10.1016/j.compositesb.2009.10.005
63. Hassan MR, Scarpa F, Mohamed NA, Ruzzene M (2008) Tensile properties of shape memory alloy chiral honeycombs. Phys Status Solidi B 245:2440–2444. https://doi.org/10.1002/pssb.200880263
64. Jiang Y, Li Y (2018) 3D printed auxetic mechanical metamaterial with chiral cells and re-entrant cores. Sci Rep 8:2397
65. Almgren RF (1985) An isotropic three-dimensional structure with Poisson's ratio = −1. J Elast 15:427–430
66. Grima JN, Oliveri L, Attard D, Ellul B, Gatt R, Cicala G (2010) Hexagonal honeycombs with Zero Poisson' s ratios and enhanced stiffness. Adv Eng Mater 2010:855–862. https://doi.org/10.1002/adem.201000140
67. Olympio KR, Gandhi F (2010) Zero Poisson's ratio cellular honeycombs for flex skins undergoing one-dimensional morphing. J Intell Mater Syst Struct 21:1737–1753
68. Rafsanjani A, Akbarzadeh A, Pasini D (2015) Snapping mechanical metamaterials under tension. Adv Mater 2015:27
69. Mitschke H, Robins V, Mecke K, Schroder-Turk G (2012) Finite auxetic deformations of plane tessellations. Proc R Soc A Math Phys Eng Sci 2012:469
70. Pozniak AA, Wojciechowski KW (2014) Poisson's ratio of rectangular anti-chiral structures with size dispersion of circular nodes. Phys Status Solidi B 251:367–374. https://doi.org/10.1002/pssb.201384256
71. Grima JN, Mizzi L, Azzopardi KM, Gatt R (2016) Auxetic perforated mechanical metamaterials with randomly oriented cuts. Adv Mater 28:385–389. https://doi.org/10.1002/adma.201503653
72. Mizzi L, Attard D, Gatt R, Pozniak AA, Wojciechowski KW, Grima JN (2015) Influence of translational disorder on the mechanical properties of hexachiral honeycomb systems. Compos Part B Eng 80:84–91. https://doi.org/10.1016/j.compositesb.2015.04.057
73. Pozniak AA, Smardzewski J, Wojciechowski KW (2013) Computer simulations of auxetic foams in two dimensions. Smart Mater Struct 2013:22. https://doi.org/10.1088/0964-1726/22/8/084009
74. Zhu H, Hobdell JR, Windle AH (2001) Effects of cell irregularity on the elastic properties of 2D Voronoi honeycombs. J Mech Phys Solids 49:857–870. https://doi.org/10.1016/S0022-5096(00)00046-6

75. Zhu HX, Thorpe SM, Windle AH (2006) The effect of cell irregularity on the high strain compression of 2D Voronoi honeycombs. Int J Solids Struct 43:1061–1078. https://doi.org/10.1016/j.ijsolstr.2005.05.008
76. Zhu HX, Windle AH (2002) Effects of cell irregularity on the high strain compression of open cell foams. Acta Mater 50:1041–1052
77. Mizzi L, Salvati E, Spaggiari A, Tan J, Korsunsky AM (2020) Highly stretchable two-dimensional auxetic metamaterial sheets fabricated via direct-laser cutting. Int J Mech Sci 167:105242. https://doi.org/10.1016/j.ijmecsci.2019.105242